THE ASTRONOMICAL JOURNAL VOLUME 105, NUMBER 1 JANUARY 1993

INTRACLUSTER DUST POLARIZATION IN THE CARINA NEBULA[1]

H. G. MARRACO[2]

Facultad de Ciencias Astronómicas y Geofísicas, Universidad Nacional de La Plata, 1900 La Plata, Argentina and Instituto de Astronomía y Física del Espacio, CONICET, Argentina

E. I. VEGA[2]

Complejo Astronómico "El Leoncito" and Instituto de Astronomía y Física del Espacio, CONICET, Argentina

F. J. VRBA

U.S. Naval Observatory, Flagstaff Station, P.O. Box 1149, Flagstaff, Arizona 86002

Received 2 June 1992; revised 18 August 1992

ABSTRACT

We have obtained new *UBVRI* polarimetric observations of 25 stars and *BV* polarimetric observations of 60 stars which are embedded in the Carina Nebula. Using these data and photometric data from the literature we have modeled and subtracted the foreground dust contribution in the color excess E_{B-V} and the visual polarization. The resulting intracluster dust component is found to have a polarization efficiency less than the maximum observed for the interstellar medium. The intracluster dust is also characterized by a ratio of E_{V-K}/E_{B-V} to $\lambda_{\max}$ higher than the canonical value for the interstellar medium. This result is consistent with the anomalous extinction for this region, reported by Tapia *et al.* [MNRAS, 232, 661 (1988a)], which increases above normal values color excess ratios that are normalized at wavelengths shorter than the *V* band.

1. INTRODUCTION

The stellar content of the clusters embedded within the Carina Nebula has been studied at visible wavelengths beginning with the pioneering work of Feinstein (1969). Later investigations by Feinstein *et al.* (1973,1976), Forte (1978), Feinstein *et al.* (1980), and Feinstein (1982) extended this work to fainter stars located in the clusters Tr 14, Tr 15, Tr 16/Cr 232, and Cr 228. The results of these studies provided some indications that the values of the measured stellar Johnson $R-I/B-V$ color ratios are abnormal. This situation generated a series of papers concerning the value of the total-to-selective absorption ratio. Herbst (1976), Thé *et al.* (1980), and Thé & Groot (1983) favored high values while Turner & Moffat (1980) suggested a value more consistent with the canonical value of about 3.15.

More recently, Smith (1987) and Tapia *et al.* (1988a) have extended photometric measurements, for most of the stars in the region, to the infrared *JHKL* bands. Both papers found anomalous extinction shortward of the visible region. The latter work further concluded that the dust responsible for the anomalous extinction is specifically intracluster and is present in all the above-mentioned clusters except Tr 15.

Marraco & Forte (1980) attempted to separate intracluster from foreground polarization and later Tapia *et al.* (1988b), using a reduced set of observations, concluded that the ratio of the average wavelength of maximum linear polarization $\overline{\lambda_{\max}}$ to that of E_{V-K}/E_{B-V} for the embedded stars does not obey the standard relation as expressed, for instance, by Whittet & van Breda (1978). In this paper we present additional polarimetric observations which are used to help separate foreground from intracluster polarization components and to investigate further the reported unusual intracluster dust properties.

2. OBSERVATIONS

Sixty high luminosity stars were observed polarimetrically in the Johnson *B* and *V* bandpasses by one of us (H.G.M.) in the years 1978 to 1980. These observations were obtained with the rotating analyzer polarimeter at La Plata Observatory using the 83 cm telescope and also at "Felix Aguilar" Observatory (San Juan) using the "Perrine" 76 cm telescope. The observing and reduction techniques are identical to those described by Feinstein & Marraco (1980). These observations are presented in Table 1 along with those of the star η Carina. Some of these observations were presented pictorially by Marraco & Forte (1980). These data provided the basic background used to choose the stars for further observation in additional bandpasses.

[1]Based on observations obtained at the Complejo Astronómico *El Leoncito*, operated under agreement among the Consejo Nacional de Investigaciones Científicas y Técnicas de la República Argentina, the Secretaría de Ciencia y Tecnología de la Nación, and the National Universities of La Plata, Córdoba and San Juan.

[2]Member of the "*Carrera del Investigador Científico*" of CONICET, Argentina.

During 1988 July a group of 12 stars belonging to Trumpler 15 was observed in five colors polarimetrically by F.J.V. using the VATPOL polarimeter at the CASLEO 2.15 m telescope. These *UBVRI* observations provided a precise determination of the foreground value of λ_{max}. Later, 13 stars, selected either because they appeared to have substantial amounts of intracluster polarization from the two-color observations or large color excesses, were observed polarimetrically in *UBVRI* by E.I.V. during 1989 May using the same equipment. Standard stars for null polarization and for the zero point of the polarization position angle are the same as those used by Clocchiatti & Marraco (1988). Both sets of *UBVRI* observations are presented in Table 2.

Spectral types for most of the bright stars in Tables 1 and 2 were obtained by N. Walborn in a series of papers begun in the 1970's. Later, Morrell *et al.* (1988) obtained observations of fainter stars. This reference contains a detailed description of all spectroscopic work in the area. The spectral types themselves, including those of Morrell *et al.* (1988), can be found in Table 1 of Tapia *et al.* (1988).

3. RESULTS

As was evident from the early results of Feinstein *et al.* (1973), the distribution of the foreground extinction in the direction of the early stars associated with the Carina Nebula increases with distance; see Fig. 11 of this reference. That figure shows that $E_{B-V}\approx 0.4$ is contributed by the foreground dust. Further analysis of the area using data from Feinstein *et al.* (1976), Forte (1978), and Feinstein *et al.* (1980) revealed that the foreground extinction ranges from $E_{B-V}\approx 0.3$ in the area of Collinder 228 to $E_{B-V}\approx 0.45$ in the area of Tr 15. Following the method employed by Serkowski (1958) for h and χ Persei, we

TABLE 1. *BV* polarimetric observations.

HD	LS	⋆	$P_V\pm\epsilon$ (%)	$\theta_V\pm\epsilon$ (deg)	$P_B\pm\epsilon$ (%)	$\theta_B\pm\epsilon$ (deg)
93161	1832	16- 90	2.28±.14	107.4±1.8	2.28±.17	108.0±2.1
	1878	16- 115	2.22±.36	91.2±4.6	2.31±.23	97.4±2.9
	1874	16- 112	1.39±.20	98.6±4.1	1.37±.19	95.7±4.0
		16- 110	2.22±.13	100.0±1.7	2.23±.25	103.3±3.2
93160	1831	16- 88	2.23±.17	112.4±2.2	2.36±.26	113.4±3.2
93205	*1849*		2.21±.11	99.0±1.4	1.92±.14	97.1±2.1
93162	1833		6.54±.15	136.3±0.7	5.73±.40	134.8±2.0
93308	1868	η Car	4.50±.12	45.3±0.8	4.36±.18	45.1±1.2
303308	*1869*	*16- 108*	3.10±.12	99.3±1.1	2.69±.13	98.8±1.3
93250	1859	16- 101	2.10±.06	115.0±0.8	1.94±.07	114.2±1.0
303311	*1851*	*16- 98*	2.27±.15	106.2±1.9	1.82±.13	109.0±2.0
	1856	16- 100	3.48±.12	106.3±1.0	3.48±.11	105.4±0.9
	1861	*16- 104*	1.97±.13	105.2±1.8	1.59±.19	108.3±3.4
93129	1819		1.93±.07	111.2±1.0	1.93±.07	111.1±1.1
	1808	14- 30	2,86±.34	129.6±3.4	2.96±.23	125.1±2.2
303316	1800		3.31±.42	124.9±3.6	2.75±.15	123.3±1.6
93204	*1847*		2.08±.18	96.8±2.5	2.23±.17	92.3±2.2
93343			2.95±.40	88.5±3.9	2.86±.39	87.6±3.9
93128	1819		2.49±.19	111.5±2.2	2.05±.19	107.7±2.7
93249	*1857*	*15- 1*	2.32±.17	116.7±2.1	2.39±.19	113.0±2.3
93403	1881		2.31±.13	105.1±1.6	2.02±.13	104.8±1.8
93420		BO Car	1.50±.13	121.1±2.5	1.59±.22	117.5±4.0
RT Car		15- 16	2.26±.11	112.7±1.4	3.23±.38	113.8±3.4
	1871	*16- 1*	1.45±.25	97.4±4.9	2.67±.31	97.0±3.3
		16- 9	3.42±.24	96.4±2.0	3.84±.34	94.9±2.5
	1844	16- 10	3.49±.29	99.0±2.4	3.33±.28	98.6±2.4
		16- 20	1.95±.35	117.8±5.1	2.18±.44	113.4±5.8
		16- 21	5.80±.37	105.9±1.8	5.47±.52	105.3±2.7
	1872	16- 34	1.39±.22	97.5±4.5	1.71±.40	102.1±6.7
	1823	14- 8	1.78±.28	121.8±4.5	1.78±.25	111.7±4.0
	1814	14- 20	2.51±.30	116.4±3.4	2.22±.32	117.5±4.1
303312	1807		2.23±.37	122.5±4.8	3.61±.37	104.3±2.9
	1827		3.33±.60	89.1±5.2	3.24±.28	86.2±2.5
92740	1761		1.87±.09	101.8±1.4	1.72±.08	105.0±1.3
92741	*1758*		2.00±.13	121.3±1.9	1.58±.12	122.4±2.2
92877			1.61±.17	110.1±3.0	1.77±.16	114.6±2.6
93027	*1804*	*C- 14*	1.20±.17	119.7±4.1	1.45±.26	120.8±5.1
93028	*1803*	*C- 27*	1.56±.17	111.2±3.1	1.18±.17	117.5±4.1
93056	*1806*	*C- 13*	1.81±.21	110.1±3.3	2.15±.20	123.9±2.7
93146	*1826*	*C- 65*	1.66±.18	119.0±3.1	1.70±.18	121.3±3.0

TABLE 1. (continued)

HD	LS	⋆	$P_V \pm \epsilon$ (%)	$\theta_V \pm \epsilon$ (deg)	$P_B \pm \epsilon$ (%)	$\theta_B \pm \epsilon$ (deg)
93421		C- 88	0.34±.32	123.6±27.3	0.26±.18	130.6±19.6
93501		*C- 96*	1.31±.22	123.6±4.8	1.22±.31	121.3±7.3
93576	1901	C- 93	1.86±.20	123.1±3.1	2.17±.23	123.5±3.0
305438	*1791*	*C- 24*	2.15±.23	103.6±3.1	1.96±.16	107.1±2.3
305524	1860	C- 7	2.29±.22	100.4±2.8	1.69±.41	90.8±6.9
305544		C- 15	0.28±.27	51.3±28.0	1.11±.21	149.3±5.4
305518	1810	C- 22	3.31±.34	98.8±3.0	3.96±.19	94.9±1.4
305525	1886	C- 98	2.83±.31	81.4±3.1	3.85±.45	82.9±3.3
93632	1907	C- 92	1.14±.15	59.4±3.8	0.87±.10	62.6±3.3
	1853	C- 12	2.95±.31	97.7±3.0	1.87±.85	88.5±13.0
93281		C- 17	2.45±.18	108.2±2.1	2.30±.23	110.0±2.8
93130	1825	C- 1	1.64±.14	102.4±2.4	1.33±.16	105.1±3.4
93131	*1817*	*C- 3*	2.19±.11	116.5±1.5	2.14±.08	116.6±1.1
305523	1845	C- 32	3.04±.25	110.2±2.4	3.25±.26	112.5±2.3
	1865	C- 39	3.08±.54	112.5±5.1	3.35±.29	121.9±2.5
93206	1839	C- 33	2.56±.09	124.4±1.0	2.37±.05	124.4±0.6
93222	1852	C- 6	0.87±.11	134.7±3.6	0.95±.13	128.6±3.9
305536	*1834*	*C- 5*	1.69±.34	112.1±5.8	1.72±.26	129.8±4.3
305520	1830	C- 4	1.74±.16	127.7±2.6	1.91±.22	127.3±3.3
93191		C- 2	0.47±.14	132.0±8.6	0.41±.25	18.6±17.0
	1883	SRN-43	5.90±.48	106.5±2.3	5.09±.48	110.8±2.7

Notes to TABLE 1

HD: Henry Draper.

LS: Luminous Stars (Stephenson & Sanduleak 1971).

⋆: Identification from Feinstein, Marraco & Muzzio (1973), Feinstein, Marraco & Forte (1976), Feinstein, Fitzgerald & Moffat (1980), and Feinstein (1982): 14-, 15-, 16- and C- indicate respectively Tr 14, Tr 15, Tr 16 and Collinder 228; SRN- from van den Bergh & Herbst (1975)

P_V, θ_V: Polarization in percent, equatorial position angle in degrees, in V.

P_B, θ_B: Polarization in percent, equatorial position angle in degrees, in B.

looked for variation of the foreground extinction with galactic latitude. We first eliminated from further study all stars determined to be foreground by the authors cited above. A few other stars were also determined to be foreground and eliminated from further study by means of isocryptic line color-excess diagrams like that depicted in Fig. 9 of Feinstein *et al.* (1973), but extended to cover the entire area under study.

Figure 1 shows a plot of E_{B-V}, obtained from the cited literature, as a function of Galactic latitude for all the stars observed which were not determined to be foreground. In order to separate foreground from intracluster extinction, we selected 22 stars which were determined to be cluster members in the photometric studies of the different clusters of the area and which appear to be least affected by reddening. These stars, which are hereafter referred to as "frontside" stars, are listed in italics in Tables 1 and 2 and are coded as squares in Fig. 1. We wish to model the variation of the effects of the foreground dust with latitude and longitude using the data from the frontside stars. Despite the fact that the frontside stars were selected so as to minimize the effects of intracluster dust, it is clear that some extent of the intracluster dust is present in their color excesses and polarizations. However, since our primary goal was to remove completely the effects of foreground dust, leaving only the extinction and polarization belonging to the intracluster dust, the removal of some intracluster dust contribution is a conservative error.

A least-squares fit of the color excesses of the 22 frontside stars to a plane of Galactic longitude, latitude (l,b) was made in order to model the effects of the foreground extinction. The resulting equation is

$$E_{B-V}(l,b)=0.08330l+0.28167b-23.374(\mathrm{mag}),$$

having a rms error of unit weight of 0.035. As expected, the variation with Galactic latitude is the most significant part of the model.

Using exactly the same set of frontside stars we modeled the foreground polarization. For this purpose we used the P_B and P_V data from Tables 1 and 2. We assumed that the foreground polarization changes only in its amount and position angle depending on stellar Galactic coordinates,

TABLE 2. *UBVRI* polarimetric observations.

HD	LS	⋆	λ (μm)	$P_\lambda \pm \epsilon$ (%)	$\theta_\lambda \pm \epsilon$ (deg)
		FO-15	0.374	2.84±0.35	142.4±3.5
			0.443	2.77±0.14	144.6±1.4
			0.563	3.53±0.09	146.5±0.7
			0.670	3.70±0.09	149.8±0.7
			0.792	3.84±0.10	151.0±0.7
305518	1810	C- 22	0.374	3.20±0.14	102.6±1.2
			0.443	3.40±0.06	101.9±0.5
			0.563	3.65±0.18	103.1±1.4
			0.670	3.25±0.04	101.8±0.4
			0.792	3.23±0.10	100.8±0.9
	1856	16-100	0.374	2.86±0.15	105.6±1.5
			0.443	3.31±0.13	104.3±1.1
			0.563	3.66±0.10	107.4±0.8
			0.670	3.70±0.13	107.4±1.0
			0.792	3.55±0.14	104.9±1.1
		16-244	0.374	5.73±0.20	159.3±1.0
			0.443	7.01±0.15	165.0±0.6
			0.563	8.47±0.08	166.8±0.3
			0.670	8.44±0.06	168.7±0.2
			0.792	8.72±0.06	170.0±0.2
		16- 21	0.374	4.86±0.15	113.7±0.9
			0.443	5.39±0.15	114.6±0.8
			0.563	6.16±0.08	108.0±0.4
			0.670	5.85±0.07	114.9±0.3
			0.792	5.84±0.10	115.3±0.5
		16- 49	0.374	2.93±0.71	113.6±6.9
			0.443	2.64±0.18	111.4±1.9
			0.563	2.80±0.18	111.9±1.8
			0.670	3.01±0.17	114.0±1.6
			0.792	2.74±0.24	118.4±2.5
	1853	C- 12	0.374	1.63±0.15	95.9±2.6
			0.443	2.14±0.06	96.6±0.8
			0.563	2.18±0.05	95.2±0.7
			0.670	2.09±0.03	92.2±0.4
			0.792	2.05±0.06	91.5±0.8
305525	1886	C- 98	0.374	2.57±0.12	86.4±1.3
			0.443	2.85±0.09	84.5±0.9
			0.563	2.81±0.06	82.4±0.6
			0.670	2.57±0.03	81.7±0.3
			0.792	2.47±0.05	80.9±0.6
93501		*C- 96*	0.374	1.37±0.06	117.6±1.2
			0.443	1.36±0.05	118.2±1.0
			0.563	1.37±0.04	119.7±0.8
			0.670	1.36±0.05	120.8±1.0
			0.792	1.20±0.05	121.4±1.2
93632	1907	C- 92	0.374	0.59±0.04	64.0±1.9
			0.443	0.77±0.02	63.0±0.7
			0.563	1.06±0.03	58.0±0.8
			0.670	1.12±0.05	58.5±1.3
			0.792	1.34±0.03	51.6±0.6

TABLE 2. (continued)

HD	LS	⋆	λ (μm)	$P_\lambda \pm \epsilon$ (%)	$\theta_\lambda \pm \epsilon$ (deg)
	1814	14- 20	0.374	2.21±0.10	115.5±1.3
			0.443	2.39±0.05	115.6±0.6
			0.563	2.38±0.05	115.8±0.6
			0.670	2.07±0.04	116.9±0.6
			0.792	2.10±0.05	116.9±0.7
	1808	14- 30	0.374	2.34±0.16	124.1±1.9
			0.443	2.97±0.07	126.1±0.7
			0.563	3.12±0.06	127.8±0.5
			0.670	2.74±0.05	129.9±0.5
			0.792	2.97±0.06	131.0±0.6
		14- 15	0.374	1.52±0.22	112.0±4.1
			0.443	1.52±0.14	113.3±2.6
			0.563	1.93±0.13	110.2±1.9
			0.670	1.65±0.09	110.8±1.6
			0.792	1.67±0.14	106.5±2.4
RT Car		15- 16	0.374	2.29±0.48	138.5±6.0
			0.443	1.54±0.09	123.8±1.7
			0.563	1.70±0.04	118.1±0.7
			0.670	2.04±0.06	115.0±0.8
			0.792	2.16±0.05	114.6±0.7
		15- 15	0.374	2.68±0.13	114.0±1.4
			0.443	3.01±0.07	113.9±0.7
			0.563	3.17±0.06	114.1±0.5
			0.670	2.88±0.05	117.9±0.5
			0.792	2.88±0.11	118.7±1.1
		15- 14	0.374	2.62±0.11	111.0±1.2
			0.443	3.09±0.08	111.1±0.7
			0.563	3.48±0.05	113.1±0.4
			0.670	3.16±0.07	114.3±0.6
			0.792	3.05±0.09	114.2±0.8
		15- 13	0.374	2.58±0.15	114.2±1.7
			0.443	2.85±0.07	111.9±0.7
			0.563	3.04±0.07	113.4±0.7
			0.670	2.88±0.07	115.8±0.7
			0.792	2.84±0.13	114.4±1.3
		15- 7	0.374	2.25±0.12	115.3±1.5
			0.443	2.60±0.08	114.9±0.9
			0.563	2.82±0.07	116.1±0.7
			0.670	2.80±0.06	117.5±0.6
			0.792	2.77±0.11	116.8±1.1
		15- 2	0.374	2.06±0.10	118.2±1.4
			0.443	2.23±0.06	115.7±0.8
			0.563	2.31±0.05	118.1±0.6
			0.670	2.18±0.04	120.7±0.5
			0.792	2.12±0.09	119.3±1.2
		15- 26	0.374	2.04±0.12	111.7±1.7
			0.443	2.48±0.06	111.5±0.7
			0.563	2.52±0.09	111.3±1.0
			0.670	2.30±0.04	114.8±0.5
			0.792	2.14±0.08	116.3±1.1

TABLE 2. (continued)

HD	LS	★	λ (μm)	$P_\lambda \pm \epsilon$ (%)	$\theta_\lambda \pm \epsilon$ (deg)
		15- 23	0.443	2.03±0.08	113.1±1.1
			0.563	2.53±0.12	112.5±1.4
			0.670	2.21±0.07	118.0±0.9
			0.792	2.16±0.08	115.5±1.1
		15- 8	0.374	2.09±0.16	116.4±2.2
			0.443	2.30±0.07	115.4±0.9
			0.563	2.49±0.07	115.2±0.8
			0.670	2.26±0.04	119.7±0.5
			0.792	2.29±0.07	118.0±0.9
93249	1857	15- 1	0.374	1.90±0.05	115.8±0.8
			0.443	1.96±0.05	114.9±0.7
			0.563	2.08±0.05	116.1±0.7
			0.670	2.26±0.03	119.4±0.4
			0.792	1.95±0.04	118.3±0.6
		15- 4	0.374	2.04±0.32	116.8±4.5
			0.443	2.37±0.08	112.8±1.0
			0.563	2.65±0.08	113.5±0.9
			0.670	2.41±0.06	116.1±0.7
			0.792	2.30±0.11	116.1±1.4
		15- 5	0.443	2.88±0.11	119.3±1.1
			0.563	2.89±0.10	120.7±1.0
			0.670	2.92±0.07	121.2±0.7
			0.792	2.92±0.12	116.6±1.2

Notes to TABLE 2

HD: Henry Draper.
LS: Luminous Stars (Stephenson & Sanduleak 1971).
★: Identification from Feinstein, Marraco & Muzzio (1973), Feinstein, Marraco & Forte (1976), Feinstein, Fitzgerald & Moffat (1980), and Feinstein (1982): 14-, 15-, 16- and C- indicate respectively Tr 14, Tr 15, Tr 16 and Collinder 228; FO- from Forte & Orsatti (1981).
λ: Wavelength in μm.
$P_\lambda, \theta_\lambda$: Polarization in percent, equatorial position angle in degrees, at λ.

but that λ_{max} remains constant over the zone under study. To obtain the value of λ_{max} for the foreground material, we used the two-color polarization ratio of Serkowski *et al.* (1975)

$$\lambda_{max}=0.49\left(\frac{P_V}{P_B}\right)^{1.95}(\mu\mathrm{m}).$$

The weighted average of P_V/P_B for the 22 frontside stars is 1.048±0.023, giving

$$\overline{\lambda_{max}}=0.536\pm0.023(\mu\mathrm{m}).$$

Additional determinations of λ_{max} and P_{max} for the 7 frontside stars observed in *UBVRI* were obtained by fitting the data to the Serkowski *et al.* (1975) relationship

$$P(\lambda)/P_{max}=\exp[-1.15\ln^2(\lambda_{max}/\lambda)].$$

The individual results are listed in Table 3, while the weighted average λ_{max} for these 7 stars is

$$\overline{\lambda_{max}}=0.565\pm0.012\ \mu\mathrm{m},$$

consistent with the two-color determinations of $\overline{\lambda_{max}}$. Combining the *BV* and *UBVRI* results we obtain for the foreground dust an average of

$$\overline{\lambda_{max}}=0.558\pm0.010\ \mu\mathrm{m}.$$

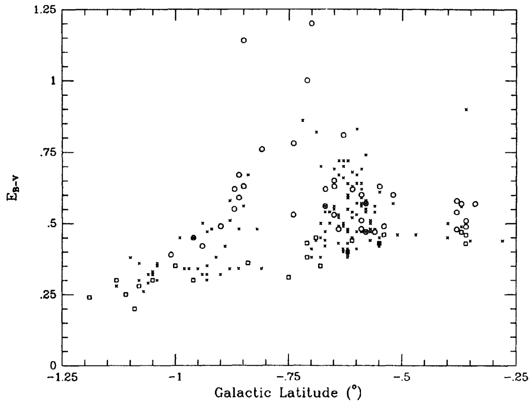

FIG. 1. The color excesses E_{B-V} as a function of Galactic latitude. (b). Nonmembers of the Carina complex were excluded as explained in the text. Small symbols indicate stars for which E_{B-V} was obtained from one of the studies of the zone but that were not observed polarimetrically. Big symbols are stars for which we have polarimetric observations: squares stand for frontside stars and circles for the remaining stars. Note the groupings at $b=-0.37$ (Tr 15), at -0.55 to -0.68 (Tr 14/16), and the dark lane at -0.78 mentioned in the text as "southeast of Tr 16."

The average $\langle P_V/P_B \rangle$ value determined above was used to obtain Q_V and U_V, the Stokes parameters of the visual foreground polarization at the position of each frontside star. The fitting of a plane to each Stokes parameter was again done by weighted least-squares to the 22 frontside stars, with the results

$$Q_V(l,b)=1.12297l-0.42011b-324.541 \quad \sigma=0.49\%$$

$$U_V(l,b)=0.72306l-0.12889b-209.408 \quad \sigma=0.43\%,$$

where σ is the rms deviation of a single star from the solution.

We are now able to subtract the effects of foreground extinction from any other object (other than the frontside stars) in the zone under study. Given Galactic coordinates, we can estimate color excess and polarimetric $P_{\max}$ and position angle for the contribution of the foreground dust at that line of sight. The foreground polarization is assumed to have the value of $\overline{\lambda_{\max}}$ determined above. Tables 4 and 5 give these results for all the stars for which we have two-color and five-color polarization data, respectively. Both tables together represent the observed polarization of the intracluster material. Note that neither Tables 4 nor 5 include data for the frontside stars, as the residual reddenings and polarizations for those stars are meaningless. Note also that the errors quoted for the intracluster polarizations in Tables 4 and 5 are internal errors. The uncertainties of 0.43% and 0.49% quoted for a single star in the least-squares solution for the foreground Q_V and U_V parameters represent a lower limit to the external polarization errors of the program stars.

The value of the ratio of polarization to absorption (P_V/A_V) depends on several factors which work simultaneously to give a final value that can be as high as 3%/mag and as little as zero. The higher value is observed when the interstellar magnetic field is (a) high enough to ensure complete alignment, (b) uniform, and (c) oriented in the plane of the sky and also when the particles that produce the extinction are prolate spheroids that produce maximum polarization efficiency. Failure of any of the above conditions lowers this value, as is also the case for multiple magnetic field components at differing position angles.

The observed and the intracluster visual polarizations are plotted vs their observed and intracluster E_{B-V} values in Fig. 2 using data extracted from Table 4. The line of maximum polarization efficiency is plotted in both graphs using $R_V=3.15$. For reference, the dotted line also drawn in the intracluster plot represents maximum polarization efficiency assuming $R_V=6$. The latter value is only one-half of the R_V (intracluster) = 12 suggested by Tapia *et al.* (1988a). While not specifically shown in these figures, the

TABLE 3. $\lambda_{\max}$ for frontside stars with 5 color data.

HD	LS	⋆	$\lambda_{max} \pm \epsilon$ (μm)
93501		*C- 96*	0.517±0.021
		14- 15	0.583±0.041
		15- 26	0.532±0.022
		15- 3	0.568±0.035
93249	*1857*	*15- 1*	0.584±0.021
		15- 4	0.565±0.021
		16- 49	0.606±0.033

Notes to TABLE 3

HD: Henry Draper.

LS: Luminous Stars (Stephenson & Sanduleak 1971).

⋆: Identification from Feinstein, Marraco & Muzzio (1973), Feinstein, Marraco & Forte (1976), Feinstein, Fitzgerald & Moffat (1980), and Feinstein (1982): 14-, 15-, 16- and C- indicate respectively Tr 14, Tr 15, Tr 16 and Collinder 228.

λ_{max}: Wavelength of maximum polarization in μm.

TABLE 4. Observed, foreground, and intracluster color excesses and visual polarizations.

HD	LS	★	E_{B-V} O	F	I	Observed $P_V \pm \epsilon$ (%)	$\theta_V \pm \epsilon$ (deg)	Foreground P_V (%)	θ_V (deg)	Intracluster $P_V \pm \epsilon$ (%)	$\theta_V \pm \epsilon$ (deg)
93161	1832	16- 90	.51	.40	.11	2.28±.14	107.4±1.8	2.12	112.4	0.41±.15	75.9±10.1
	1878	16-115	.48	.41	.07	2.22±.36	91.2±4.6	1.84	113.4	1.58±.38	63.7± 6.9
	1874	16-112	.65	.40	.25	1.39±.20	98.6±4.1	1.84	113.5	0.94±.21	47.2± 6.4
		16-110	.63	.40	.23	2.22±.13	100.0±1.7	1.84	113.5	1.02±.13	72.5± 3.7
93160	1831	16- 88	.48	.40	.08	2.23±.17	112.4±2.2	2.12	112.4	0.10±.17	112.7±47.1
93162	1833		.70	.38	.32	6.54±.15	136.3±0.7	1.99	113.0	5.37±.15	144.1± 0.8
93308	1868	η Car	.40	.41	.00	4.50±.12	45.3±0.8	1.90	113.2	6.01±.13	38.9± 0.6
93250	1859	16-101	.49	.42	.07	2.10±.06	115.0±0.8	2.05	112.5	0.19±.06	151.0± 8.8
	1856	16-100	.53	.37	.16	3.66±.10	107.4±0.8	1.86	113.6	1.89±.10	101.3± 1.5
93129	1819		.47	.42	.05	1.93±.07	111.2±1.0	1.94	112.9	0.12±.07	62.4±17.2
	1808	14- 30	.81	.39	.42	3.12±.06	127.8±0.6	2.19	112.3	1.68±.06	148.8± 1.0
303316	1800			.34		3.31±.42	124.9±3.6	2.08	112.8	1.65±.41	140.5± 7.2
93343			.62	.40	.22	2.95±.40	88.5±3.9	1.75	113.8	2.29±.40	70.4± 5.0
93128	1819		.57	.40	.17	2.49±.19	111.5±2.2	2.17	112.3	0.33±.19	106.7±16.5
93403	1881		.57	.48	.09	2.31±.13	105.1±1.6	2.09	112.1	0.58±.13	74.7± 6.4
93420		BO Car		.47		1.50±.13	121.1±2.5	1.98	112.5	0.71±.13	3.0± 5.3
RT Car		15- 16	.50	.46	.04	1.70±.04	118.0±0.7	2.21	111.9	0.66±.04	5.1± 1.7
		16- 9	.53	.40	.13	3.42±.24	96.4±2.0	1.86	113.4	2.14±.24	81.9± 3.2
	1844	16- 10	.62	.41	.21	3.49±.29	99.0±2.4	1.89	113.2	2.03±.29	85.9± 4.1
		16- 21	.78	.37	.41	6.16±.08	108.0±0.4	1.86	113.6	4.35±.08	105.7± 0.5
	1872	16- 34	.56	.40	.16	1.39±.22	97.5±4.5	1.83	113.5	0.98±.22	47.7± 6.4
	1823	14- 8	.47	.41	.06	1.78±.28	121.8±4.5	2.17	112.2	0.77±.28	177.4±10.5
	1814	14- 20	.60	.40	.20	2.38±.05	115.7±0.6	2.19	112.2	0.34±.05	142.1± 4.2
303312	1807		.63	.41	.22	2.23±.37	122.5±4.8	2.28	111.9	0.83±.37	164.1±12.7
	1827		.60	.42	.18	3.33±.60	89.1±5.2	2.22	112.0	2.39±.60	68.3± 7.2
92740	1761			.31		1.87±.09	101.8±1.4	2.37	112.1	0.91±.09	45.3± 2.8
92741	1758			.25		2.00±.13	121.3±1.9	2.09	113.4	0 58±.13	166.7± 6.5
92877			.22	.28	.06	1.61±.17	110.1±3.0	2.04	113.3	0.48±.17	34.5±10.2
93146	1826	C- 65		.29		1.66±.18	119.0±3.1	1.65	115.1	0.22±.18	160.7±23.0
93421		C- 88		.32		0.34±.32	123.6±27.3	1.32	117.3	1.00±.32	25.2± 9.2
93576	1901	C- 93	.55	.37	.18	1.86±.20	123.1±3.1	1.32	116.9	0.63±.20	136.5± 9.1
305524	1860	C- 7	.63	.35	.28	2.29±.22	100.4±2.8	1.73	114.3	1.11±.22	77.1± 5.7
305544		C- 15	.00	.28	.28	0.28±.27	51.3±28.0	1.75	114.7	1.93±.27	28.0± 4.0
305518	1810	C- 22	.76	.35	.41	3.65±.18	103.1±1.4	1.95	113.3	1.95±.18	92.8± 2.6
305525	1886	C- 98	1.00	.40	.60	2.81±.06	82.4±0.6	1.62	114.5	2.57±.06	65.0± 0.7
93632	1907	C- 92	.62	.37	.25	1.06±.03	57.9±0.8	1.26	117.4	2.00±.03	41.2± 0.4
	1853	C- 12	1.14	.35	.79	2.19±.05	95.1±0.7	1.75	114.2	1.35±.05	68.5± 1.1
93281		C- 17		.35		2.45±.18	108.2±2.1	1.67	114.6	0.90±.16	95.9± 5.2
93130	1825	C- 1	.59	.34	.25	1.64±.14	102.4±2.4	1.85	113.8	0.72±.13	54.9± 5.2
305523	1845	C- 32	.49	.33	.16	3.04±.25	110.2±2.4	1.72	114.5	1.37±.28	104.7± 5.8
	1865	C- 39	.67	.35	.32	3.08±.54	112.5±5.1	1.68	114.6	1.41±.51	110.0±10.5
93206	1839	C- 33	.42	.32	.10	2.56±.09	124.4±1.0	1.69	114.7	1.12±.09	139.4± 2.3
93222	1852	C- 6	.39	.31	.08	0.87±.11	134.7±3.6	1.58	115.5	1.05±.11	9.9± 3.0
305520	1830	C- 4	.45	.32	.13	1.74±.16	127.7±2.6	1.72	114.6	0.78±.32	165.6±11.8
93191		C- 2	.05	.35	.30	0.47±.14	132.0±8.6	1.78	114.1	1.42±.25	18.5± 5.0
	1883	SRN-43	.57	.37	.20	5.90±.48	106.5±2.3	1.56	115.2	4.44±.47	103.5± 3.0
		FO- 15	1.20	.40	.80	3.52±.09	146.5±0.7	1.72	114.1	3.20±.09	161.1± 0.8
		16-244		.38		8.46±.08	166.8±0.3	1.98	113.0	9.25±.08	172.7± 0.2
	1855	15- 15	.48	.46	.02	3.17±.06	114.1±0.5	2.24	111.7	0.95±.06	119.7± 1.8
		15- 14	.54	.46	.08	3.48±.05	113.1±0.4	2.24	111.7	1.24±.05	115.5± 1.2
		15- 13	.58	.46	.12	3.04±.07	113.4±0.7	2.24	111.7	0.81±.07	118.1± 2.5
		15- 7	.57	.46	.11	2.82±.07	116.1±0.7	2.25	111.7	0.69±.07	131.0± 2.9
		15- 2	.49	.47	.02	2.30±.05	118.0±0.6	2.25	111.7	0.50±.05	156.8± 2.9
		15- 23	.51	.46	.05	2.53±.12	112.5±1.4	2.30	111.6	0.24±.12	121.6±14.3

Notes to TABLE 4

HD: Henry Draper.
LS: Luminous Stars (Stephenson & Sanduleak 1971).
★: Identification as in Tables 1, 2 and 3.
E_{B-V}: $B-V$ color excess.
O, F, I: Observed, Foreground (computed from position), Intracluster.
P_V, θ_V: Polarization in percent, equatorial position angle in degrees, in V.

TABLE 5. *UBVRI* intracluster polarization.

HD	LS	★	λ (μm)	$P_\lambda \pm \epsilon$ (%)	$\theta_\lambda \pm \epsilon$ (deg)
		FO- 15	0.374	2.37±0.35	157.5±4.2
			0.443	2.44±0.14	162.3±1.6
			0.563	3.20±0.09	161.0±0.8
			0.670	3.54±0.09	163.0±0.7
			0.792	3.71±0.10	162.4±0.8
305518	1810	C- 22	0.374	1.79±0.14	92.9±2.2
			0.443	1.85±0.06	90.6±0.9
			0.563	1.95±0.18	92.9±2.6
			0.670	1.69±0.04	88.9±0.7
			0.792	1.84±0.10	89.4±1.5
	1856	16-100	0.374	1.44±0.15	97.0±3.0
			0.443	1.74±0.13	95.0±2.1
			0.563	1.89±0.10	101.3±1.5
			0.670	1.99±0.13	101.8±1.9
			0.792	2.07±0.14	98.1±1.9
		16-244	0.374	6.03±0.20	167.2±0.9
			0.443	7.68±0.15	171.8±0.6
			0.563	9.26±0.08	172.7±0.2
			0.670	9.31±0.06	174.2±0.2
			0.792	9.55±0.06	174.7±0.2
		16- 21	0.374	3.31±0.15	113.7±1.3
			0.443	3.64±0.15	115.1±1.2
			0.563	4.35±0.08	105.6±0.5
			0.670	4.06±0.07	115.5±0.5
			0.792	4.23±0.10	115.9±0.7
	1853	C- 12	0.374	0.98±0.15	64.9±4.4
			0.443	1.24±0.06	71.6±1.4
			0.563	1.34±0.05	68.5±1.1
			0.670	1.46±0.03	65.7±0.6
			0.792	1.46±0.06	67.6±1.2
305525	1886	C- 98	0.374	2.14±0.12	70.6±1.6
			0.443	2.47±0.09	68.4±1.0
			0.563	2.56±0.06	65.0±0.7
			0.670	2.39±0.03	63.5±0.4
			0.792	2.32±0.05	63.9±0.6
93632	1907	C- 92	0.374	1.34±0.04	39.8±0.9
			0.443	1.61±0.02	40.9±0.4
			0.563	2.00±0.03	41.2±0.4
			0.670	2.00±0.05	42.3±0.7
			0.792	2.22±0.03	40.8±0.4
	1814	14- 20	0.374	0.45±0.10	129.3±6.3
			0.443	0.42±0.05	133.2±3.4
			0.563	0.34±0.05	142.3±4.2
			0.670	0.34±0.04	162.7±3.4
			0.792	0.38±0.05	144.0±3.7
	1808	14- 30	0.374	0.99±0.16	147.8±4.6
			0.443	1.49±0.07	146.0±1.3
			0.563	1.68±0.06	148.9±1.0
			0.670	1.58±0.05	154.9±0.9
			0.792	1.86±0.06	150.2±0.9

TABLE 5. (continued)

HD	LS	⋆	λ (μm)	$P_\lambda \pm \epsilon$ (%)	$\theta_\lambda \pm \epsilon$ (deg)
		15- 16	0.374	1.89±0.48	164.0±7.2
			0.443	0.91±0.09	180.5±2.8
			0.563	0.66±0.04	185.1±1.7
			0.670	0.24±0.06	168.9±7.1
			0.792	0.31±0.05	132.6±4.6
	1855	15- 15	0.374	0.84±0.13	119.1±4.4
			0.443	0.92±0.07	118.9±2.2
			0.563	0.96±0.06	119.7±1.8
			0.670	0.90±0.05	133.3±1.6
			0.792	1.10±0.11	131.4±2.9
		15- 14	0.374	0.76±0.11	109.3±4.1
			0.443	0.98±0.08	109.8±2.3
			0.563	1.25±0.05	115.6±1.1
			0.670	1.03±0.07	119.8±1.9
			0.792	1.12±0.09	118.5±2.3
		15- 13	0.374	0.74±0.15	120.5±5.8
			0.443	0.74±0.07	112.5±2.7
			0.563	0.82±0.07	118.1±2.4
			0.670	0.81±0.07	127.0±2.5
			0.792	0.92±0.13	120.1±4.0
		15- 7	0.374	0.46±0.12	130.7±7.4
			0.443	0.55±0.08	127.6±4.1
			0.563	0.69±0.07	131.1±2.9
			0.670	0.81±0.06	133.8±2.1
			0.792	0.91±0.11	127.9±3.4
		15- 2	0.374	0.48±0.10	148.5±5.9
			0.443	0.32±0.06	148.4±5.3
			0.563	0.51±0.05	156.5±2.8
			0.670	0.68±0.04	160.6±1.7
			0.792	0.56±0.09	152.0±4.6
		15- 23	0.443	0.17±0.08	182.6±3.4
			0.563	0.24±0.12	121.2±4.2
			0.670	0.49±0.07	160.0±4.1
			0.792	0.33±0.08	143.6±6.9
		15- 5	0.443	0.99±0.11	136.5±3.2
			0.563	1.01±0.10	142.6±2.8
			0.670	1.11±0.07	141.1±1.8
			0.792	1.03±0.12	126.1±3.3

Notes to TABLE 5

HD: Henry Draper.
LS: Luminous Stars (Stephenson & Sanduleak 1971).
⋆: Identification as in Tables 1, 2, and 3.
λ: Wwavelength in μm.
$P_\lambda, \theta_\lambda$: Polarization in percent, equatorial position angle in degrees, at λ.

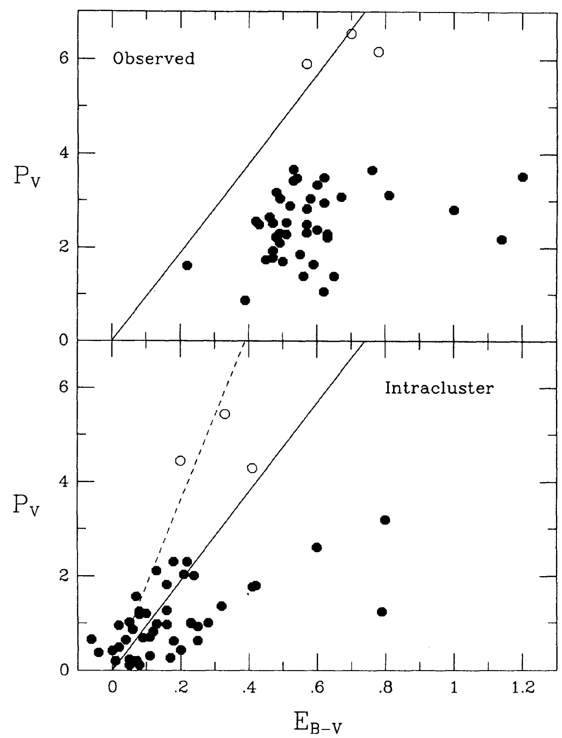

FIG. 2. Polarization efficiency diagrams for both observed and intracluster dust. Using $R_V=3.15$, the line of maximum efficiency is drawn in both diagrams. In the intracluster plot a dotted line is also included for maximum efficiency using $R_V=6$. The three stars coded with open symbols are likely intrinsically polarized and are discussed in the text.

polarization efficiency of foreground material is found to be intermediate, as is frequently the case for lines of sight of more than 2 kpc directed at $l=289°$.

The plot of intracluster polarization versus E_{B-V} demonstrates the success of our conservative selection of frontside stars; many of the low extinction stars are near the line of maximum efficiency. Stars more deeply immersed in the dust lanes of the area divide into two groups: those of high polarization and those of high extinction. The former group, coded with open symbols, is composed of three stars (SRN 43, HD 93162, and Tr 16–21), which are likely intrinsically polarized. SRN 43 is an emission-line star (Herbst 1975), HD 93162 is a well known WR star, and Tr 16–21 shows variations of polarization position angle, as will be discussed later. The stars with high extinction are located in the dust lane to the east and south of Tr 16 and between that cluster and Cr 228. The magnetic field is probably somewhat tilted in relation to the plane of the sky in that lane. No conclusion can be extracted from these diagrams with regard to the E_{B-V} "deficiency" of Tapia *et al.* (1988a), but they strongly argue against a value of $R_V \geqslant 6$.

Table 6 contains results for those nonfrontside stars with five-color polarimetric data. The rotation of the polarization position angle as a function of wavelength can be interpreted as (a) the combination of two interstellar contributions with different position angles and different values of λ_{max}, (b) the combination of interstellar polarization with intrinsic polarization differing in both position angle and wavelength dependence, or (c) the superposition of (a) and (b). If our model for the foreground polarization reasonably represents one of the interstellar contributions in case (a) above, then the derived intracluster polarization should show less position angle rotation than the observed results, unless cases (b) and (c) also play important roles.

In order to check for the above cases, we have computed the dispersion of position angle for each star, σ_θ, and normalized it by the average of the position angle errors, $\bar{\epsilon}$, for both observed and intracluster data. The results are included in Table 6. Such a ratio, if no significant rotation of polarization position angle is present, and, hence, none of the above cases are operative, should be close to unity. Our results show that stars Cr−22, Tr16−100, Tr15−13, and Tr15−7 have no position angle rotation; stars FO−15 Cr−12, Cr−92, and Tr15−2 are of case (a), stars Tr16−21, Cr−98, Tr15−16 (RT Car), Tr15−15, Tr15 −14, and Tr15−5 are of case (b), and stars Tr16−244 and Tr14−30 are of case (c). These conclusions are based on the truth table shown in Table 7. Two stars, flagged with colons in the intracluster column, have computed intracluster $P_{max} < 0.5\%$ and, hence, small intracluster polariza-

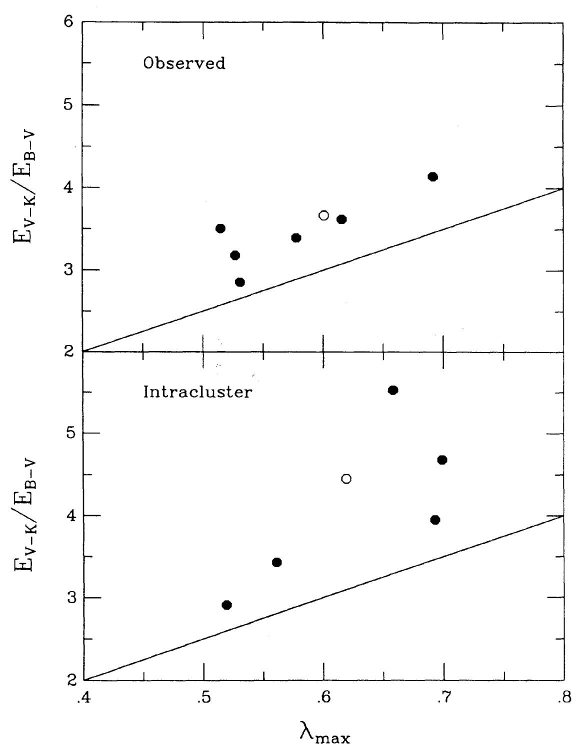

FIG. 3. The wavelength of maximum polarization, λ_{max}, vs the color excess ratio E_{V-K}/E_{B-V} for both observed and intracluster dust. A normal $E_{V-K}/E_{B-V}=2.80$ was used to substract the foreground excesses. The canonical relation corresponding to $R_V=5.6\lambda_{max}$ is shown as a line in both plots. The likely intrinsically polarized star Tr 16-21 is coded with an open symbol.

TABLE 6. *UBVRI* polarization results.

HD	LS	★	$\sigma_\theta/\bar{\epsilon}$ O	$\sigma_\theta/\bar{\epsilon}$ I	Observed $\lambda_{max}\pm\epsilon$ (μm)	Observed $P_{max}\pm\epsilon$ (%)	Observed σ_1 (%)	Intracluster $\lambda_{max}\pm\epsilon$ (μm)	Intracluster $P_{max}\pm\epsilon$ (%)	Intracluster σ_1 (%)
		FO- 15	2.24	1.22	.726±.033	3.80±.10	0.42	.786±.031	3.66±.10	0.36
305518	1810	C- 22	0.89	1.06	.531±.021	3.53±.08	0.66	.519±.038	1.89±.08	1.20
	1856	16-100	1.16	1.24	.616±.008	3.75±.03	0.13	.658±.026	2.03±.06	0.39
		16-244	8.22	6.32	.692±.022	8.73±.13	0.40	.699±.019	9.58±.12	0.34
		16- 21	4.70	4.64	.601±.020	6.12±.10	0.38	.619±.031	4.29±.11	0.57
	1853	C- 12	1.92	1.37	.570±.026	2.20±.05	0.88	.675±.026	1.46±.03	0.73
305525	1886	C- 98	2.67	3.23	.527±.027	2.82±.09	0.92	.561±.024	2.54±.06	0.76
93632	1907	C- 92	4.09	1.47	.877±.023	1.32±.05	1.16	.734±.020	2.18±.06	1.17
	1814	14- 20	0.85	2.76:	.515±.031	2.40±.09	1.38	.506±.072	0.40±.04	3.25
	1808	14- 30	2.93	1.71	.578±.047	3.07±.13	1.37	.693±.065	1.74±.09	1.59
RT Car		15- 16	4.53	3.93	.814±.077	2.10±.14	1.48	.229±.083	1.50:	5.63
		15- 15	2.55	2.52	.540±.021	3.13±.06	0.58	.578±.055	0.98±.04	1.44
		15- 14	1.89	1.84	.581±.020	3.38±.06	0.53	.641±.065	1.17±.07	1.52
		15- 13	1.28	1.34	.564±.015	3.05±.04	0.35	.613±.046	0.85±.04	0.97
		15- 7	0.98	0.57	.602±.014	2.87±.03	0.33	.812±.039	0.85±.05	0.69
		15- 2	1.83	1.17	.541±.016	2.33±.04	0.55	.855±.182	0.66±.14	3.94
		15- 23	1.96	2.33:	.608±.034	2.31±.07	0.69	1.12±.360	0.49±.23	3.99
		15- 5	2.31	2.32	.590±.038	3.03±.09	0.59	.626±.039	1.10±.03	0.57

Notes to TABLE 6

HD: Henry Draper.
LS: Luminous Stars (Stephenson & Sanduleak 1971).
★: Identification as in Tables 1, 2, and 3.
$\sigma_\theta/\bar{\epsilon}$: See text.
O, I: Observed, intracluster.
λ_{max}: Wavelength of maximum polarization in μm.
P_{max}: Polarization at λ_{max} in percent.
σ_1: Unit weight error of fit.

tions in relation to the external errors. We have chosen not to extract results from these stars.

The $\lambda_{\max}$ and $P_{\max}$ listed in the following columns of Table 6 were obtained using a weighted least-squares fit to the Serkowski *et al.* (1975) relation. A column is included for both the observed and intracluster fits that gives the unit weight error, σ_1. Due to the weighting scheme that was used, this quantity should not be higher than 2 if the polarization is well represented by the Serkowski relation.

For those stars that have intracluster $P_{\max}\geqslant 0.5\%$, σ_1 lower than 2, and which have been observed in the *JHK* by Tapia *et al.* (1988a), we have plotted in Fig. 3 both the observed and the intracluster $\lambda_{\max}$ versus the color excess ratio E_{V-K}/E_{B-V}. Whittet & van Breda (1978) determined, for grains in the general interstellar medium, what we here term the *canonical* relation between these quantities, $R_V=A_V/E_{B-V}=5.6\lambda_{\max}$. In terms of E_{V-K}/E_{B-V} this results in

$$\frac{E_{V-K}}{E_{B-V}}=\frac{A_V/E_{B-V}}{A_V/E_{V-K}}=\frac{R_V}{A_V/E_{V-K}}=\frac{5.6\lambda_{\max}}{1.12}\simeq 5.0\lambda_{\max}.$$

In both parts of Fig. 3 the *canonical* ratio of 5.0 is drawn as a solid line.

The observed points appear to follow a strip nearly parallel to, but above, the *canonical* line. Since foreground color excess ratios were found to be normal, $E_{V-K}/E_{B-V}=2.80$, by Tapia *et al.* (1988a), and a normal foreground value of $\lambda_{\max}=0.56$ μm was found in this study, the foreground dust contribution is at the *canonical* ratio. When the normal foreground dust component is removed, the resultant intracluster data points scatter well above the *canonical* line, as is seen in the bottom panel of Fig. 3. Even not considering the star Tr 16−21 (coded by an open symbol), which may be intrinsically polarized, it is clear that for the intracluster dust the canonical relation, $E_{V-K}/E_{B-V}=5.0(\lambda_{\max})$, is not valid, as previously shown by Tapia *et al.* (1988b). This high ratio and scatter are most likely due to the anomalous extinction for this region, reported by Tapia *et al.* (1988a), which increases the color excess ratios that are normalized at wavelengths shortward of the *V* band.

4. CONCLUSIONS

The foreground polarization in the direction of the area under study is normal and has a $\lambda_{\max}$ of 0.56 μm. Its direction is slowly variable over the area but averages 112°

TABLE 7. $\sigma_\theta/\bar{\epsilon}$ truth table.

in equatorial coordinates, while the amount varies between 1.2% and 2.2%, increasing toward lower Galactic latitudes. Polarization efficiency is intermediate.

The intracluster polarization is characterized by a higher than normal value of λ_{max}, but which does not exceed 0.78 μm (star FO−15). Polarization efficiency is lower than the maximum observed for the interstellar medium, especially in the dust lane that is located southeast of Tr 16.

The conclusion of Tapia *et al.* (1988a) are supported: the Carina Nebula has anomalous extinction in that the canonical λ_{max} vs R_V relation is not followed when R_V is defined as normalized by E_{B-V}.

REFERENCES

Clocchiatti, A., & Marraco, H. G. 1988, A&A, 197, L1
Feinstein, A. 1969, MNRAS, 143, 273
Feinstein, A. 1982, AJ, 87, 1012
Feinstein, A., Fitzgerald, M. P., & Moffat, A. F. J. 1980, AJ, 85, 708
Feinstein, A., & Marraco, H. G. 1980, PASP, 92, 266
Feinstein, A., Marraco, H. G., & Forte, J. C. 1976, A&AS, 24, 389
Feinstein, A., Marraco, H. G., & Muzzio, J. C. 1973, A&AS, 12, 331
Forte, J. C. 1978, AJ, 83, 1199
Herbst, W. 1975, AJ, 80, 212
Herbst, W. 1976, ApJ, 208, 923
Marraco, H. G., & Forte, J. C. 1980, in Star Clusters, IAU Symposium No. 85, edited by J. E. Hesser (Reidel, Dordrecht), p. 241
Morrell, N., Garcia, B., & Levato, H. 1988, PASP, 100, 1431
Serkowski, K. 1958, AcA, 8, 135
Serkowski, K., Mathewson, D. S., & Ford, V. L. 1975, ApJ, 196, 261
Smith, R. G. 1987, MNRAS, 227, 943
Tapia, M., Roth, M., Marraco, H., & Ruiz, M. T. 1988a, MNRAS, 232, 661
Tapia, M., Roth, M., Marraco, H., & Ruiz, M. T. 1988b, in Conference on Dust in the Universe, edited by M. E. Bailey and D. A. Williams (Cambridge University Press, Cambridge), p. 19
Thé, P. S., & Groot, M. 1983, A&A, 125, 75
Thé, P. S., Tjin, A., Djie, H. R. E., Kudritzki, R. P., & Wesselius, P. R. 1980, A&A, 91, 360
Turner, D. G., & Moffat, A. F. J. 1980, MNRAS, 192, 283
Whittet, D. C. B., & van Breda, I. G. 1978, A&A, 66, 57